Kinetic Modeling of Methanol-to-Olefin Reaction over ZSM-5 in Fluid Bed

Mads Kaarsholm,*,† Banafsheh Rafii,† Finn Joensen,‡ Roberta Cenni,‡ Jamal Chaouki,† and Gregory S. Patience†

Department of Chemical Engineering, École Polytechnique de Montréal, Canada, and Haldor Topsøe A/S, Denmark

The methanol to olefins reaction has been studied in a small scale fluidized bed reactor over a phosphorus modified ZSM-5 catalyst. The product distribution was relatively insensitive to either feed rate or inlet gas composition. It was more sensitive to temperature with a significant increase in light olefins when the temperature was increased from 400 to 550 °C. A model based on the hydrocarbon pool mechanism is proposed in which olefins form through reversible reactions with a high molecular weight hydrocarbon species in catalyst pores and intersections. Agreement between the model and the product distribution of the olefinic species is good throughout the temperature interval investigated. Further experimental work is required to adequately characterize the paraffin and C_{6+} fractions.

Introduction

The methanol-to-olefin (MTO) reaction over acid zeolites was first discovered in the late 1970s by researchers at Mobil when trying to convert methanol over ZSM-5 to other oxygenated compounds.[1] Large efforts have since been taken to optimize the reaction with respect to both olefin and gasoline production. Stöcker[2] gave an excellent review of different catalysts with respect to pore size, zeolite types, and effects of zeolite modifications with different metals.

ZSM-5 and SAPO-34 are among the most intensively studied catalysts for methanol conversion. The main difference between the two catalysts is the pore and cage structure: SAPO-34 has narrow pores with a diameter of 3.8 Å and large cages. Larger aromatic compounds are therefore allowed to form inside the cages but the narrow pores inhibit aromatic intermediates from exiting. ZSM-5 has larger pores with diameters of 5.1−5.6 Å where larger molecules—like aromatics—can escape. SAPO-34, therefore, has a narrow product distribution of C_1-C_5 hydrocarbons while ZSM-5 gives products in the range of C_1-C_{10}. Because of the accumulation of large aromatic species inside the cages of SAPO-34, the catalyst deactivates much faster than ZSM-5.[2]

Interpreting experimental data derived from fixed bed reactors for the MTO reaction is complicated due to the possibility of radial and axial gradients of temperature, gas phase composition as well as carbon deposition on the catalyst.[3−7] Spatial uniformity of the particulate phase is one of the major advantages of studying kinetics in a fluidized bed. Thus, coking of the pores will be uniform. Furthermore, fluidized beds operate isothermally, which is an important consideration for highly exothermic reactions like MTO. Although selectivity may be compromised because of backmixing in fluidized beds several investigations of both SAPO-34 and ZSM-5 zeolites[8−11] indicate good selectivity of the MTO reaction. Constant catalyst activity and product distribution can also be obtained by continuous regeneration.

Kinetic modeling of the MTO reaction has been the focus of many studies over the years. Stöcker[2] summarized the work on the pathway for the first C−C bond that has been disputed for years while Keil[10] reviewed models based on lumping species together. Detailed models have also been developed.[12−14] Recently the group of Bilbao at Universidad del Pais Vasco have collected an extensive amount of experimental data and modeled the MTO/MTG reaction kinetics and deactivation for both ZSM-5 and SAPO catalysts.[5,6,8,15−17] This work has been reasonably successful in characterizing deactivation both as function of time on stream and regeneration. The modeling has mainly been focused on lumped fractions except for SAPO-34 catalyst where the olefinic species distribution was characterized considering the hydrocarbon pool mechanism.[17] Part and Froment[18] developed a kinetic model based on elementary steps of carbenium ion chemistry in which ethylene and propylene are the main products from methanol and dimethyl ether (DME) and with equilibrium reactions from C_4 to C_8 olefins. Schoenfelder et al.[9] developed a kinetic model for MTO over ZSM-5 that predicts ethylene, propylene, and butylenes while lumping the paraffins and higher olefins. The propylene and butylenes are formed by reaction with lower olefins and methanol. The model predicts the experimental data well, but higher hydrocarbons than butylenes were not quantified in the experimental work and, therefore, were incorporated with the aromatics fraction. Previous work on kinetic models generally neglected cracking of olefins or excluded propylene and ethylene oligorimerization/cracking reactions, though Bos et al.[19] included direct reactions from both butylenes and propylene to ethylene. Buchanan et al.[20] performed experiments of olefin cracking over ZSM-5 at 510 °C with $C_{5=}$ to $C_{8=}$ olefins and showed that $C_{5=}$ cracked to ethylene, propylene, and some butylenes while the higher olefins predominantly cracked to $C_{3=}$ to $C_{5=}$ olefins. These reactions have been shown to be relatively fast at this temperature, and it was necessary to include them in the reaction pool in order to model MTO correctly. Zhou at al.[21] reacted ethylene, propylene, and *n*-butylene over SAPO-34 at 450 °C in a small scale fixed-bed reactor with a weight hourly space velocity (WHSV) ranging from 1 to 424 h^{-1}. They showed that the resulting product distribution was close to equilibrium and proposed a kinetic model where all olefins were in equilibrium with a carbenium ion lump. The model was able to reproduce their results fairly well.

In this work, experimental data from the MTO reaction over a phosphorus-modified ZSM-5 catalyst conducted in a small scale fluid bed will be presented. On the basis of available literature studies and experiments using 1-hexene as feed, a

* To whom correspondence should be addressed. Tel.: + 45 45 27 22 55. E-mail: mkaa@topsoe.dk.
† École Polytechnique de Montréal.
‡ Haldor Topsøe A/S.

10.1021/ie900341t
Published on Web 11/23/2009

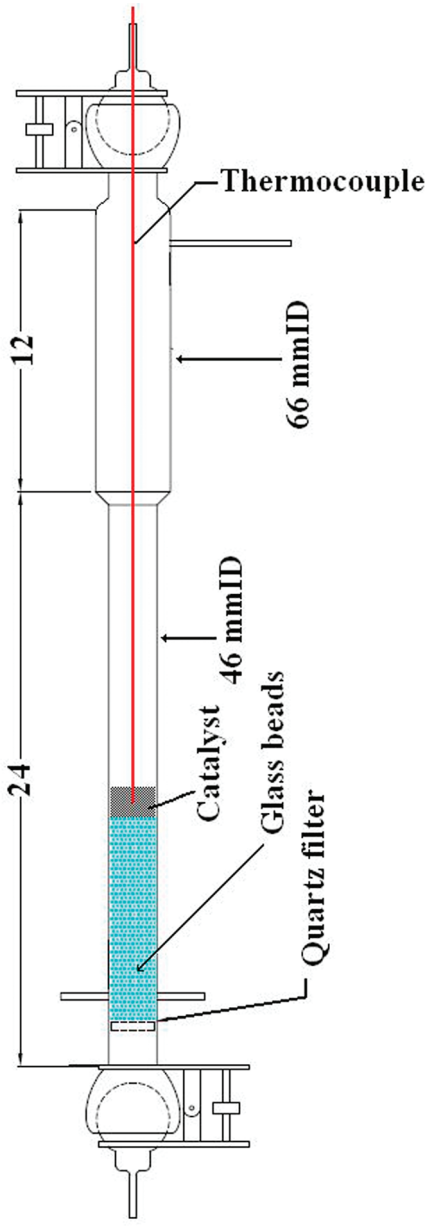

Figure 1. Drawing of the glass fluid-bed reactor. Glass beads are used to elevate the catalyst for catalyst amounts below 100 g.

kinetic model is proposed. The model is based on the hydrocarbon pool mechanism where the olefins are formed through reversible reactions with large hydrocarbon species. The fluidized bed is modeled as a two phase system with a bubble and an emulsion phase with reaction only in the emulsion phase.

Experimental Details

Equipment. MTO experiments were carried out in a 0.046 m inner diameter glass fluid bed (Figure 1) with a 0.066 m inner diameter disengagement zone. The gas was distributed through a quartz frit. The reactor was heated by two electrical band heaters: one in the reaction zone and one in the disengagement zone. Both were controlled based on thermocouples mounted on the exterior surface of the quartz reactor. A thermocouple inserted in the middle of the reaction zone recorded the temperature. Liquid feed was delivered via a dual piston pump with feed steps of 0.01 mL/min and gas was fed from one of two lines both controlled by Brooks mass flow controllers with a maximum flow rate of 2 NL/min. The selection of the reactor feed gas—methanol/inert, air, or purge gas—was made using an 8-port Valco valve. The feed was preheated by passing it through a stainless steel coil immersed in a sand bath at 200 °C followed by a heated line that was maintained at 120−150 °C. All flows and reactor temperatures were controlled by a computer. The exit gas was analyzed by a Hiden MS QIC-20 and a Varian CP3800 GC. A diagram of the system is shown in Figure 2.

Catalyst. The catalyst was composed of 10% CBV28014 (Zeolyst) imbedded in a Si/Al matrix consisting of Catapal B, Levasil 100s/30%, and kaolin. It was spray dried then calcined in air at 550 °C for 4 h. Methane formation was problematic owing to the Catapal, Levasil, and kaolin. Therefore, the powder was slurried together with an aqueous $(NH_3)_2HPO_4$ solution and then dried and calcined. The resulting catalyst contained 1.5% phosphorus and had an average particle size of 108 μm. By this treatment methane production was significantly reduced.

The particle size distribution was measured on a Horiba LA-950 particle-size analyzer. The minimum fluidization velocity at ambient temperature and pressure was 0.0051 m/s in a 0.076 m transparent fluid bed where the tapped particle density and density at minimum fluidization were also measured. The catalyst properties are listed in Table 1.

Experimental Conditions. The fluid-bed reactor was loaded with 20−330 g of catalyst. The heating elements were positioned 4 cm above the distributor, and the temperature control of the catalytic bed was therefore not optimal for inventories less than 100 g. With larger inventories the temperature just above the distributor was measured to ensure that the temperature gradient over the bed was low (between 3 and 7 °C). For experiments conducted with less than 100 g of catalyst, glass beads were used to elevate the bed into the heating zone. Cold flow experiments in a transparent fluid bed were made prior to the MTO experiments to examine the mixing behavior of the beads and catalyst. As long as the gas velocity was kept below the minimum fluidization velocity ($\mathbf{u}_{mf}$) of the beads, mixing between the beads and the catalyst was negligible and most of the catalyst remained on top. When the gas velocity was increased above $\mathbf{u}_{mf}$, the beads and catalyst would form a homogeneous mixture. A large fraction of the small particles would form a bed above the large particles when the gas velocity was subsequently reduced (some of the small particles tended to stay at the bottom of the fluid bed). In all experiments, the superficial gas velocity was maintained below $\mathbf{u}_{mf}$ of the glass beads thereby ensuring the catalyst remained above the beads.

The feed consisted of pure methanol and mixtures of methanol with water or argon. The total flow rates ranged from 0.5 to 3.6 NL/min corresponding to superficial gas velocities between 1.3 and 10 cm/s at operating conditions. All experiments were conducted between 400 and 550 °C. Blank experiments confirmed that decomposition of methanol was minimal; only minor amounts of DME were detected.

Experimental Data. Prior to studying the MTO kinetics, the stability of the catalyst with regard to the product distribution was tested in order to establish the influence of coking on activity. An experiment carried out at a WHSV of 2.4 h^{-1} with pure methanol at 550 °C showed that the product distribution was stable for the first 15 h in the fluid bed. In other experiments, performed at 450, 500, and 550 °C with a WHSV of 0.4 h^{-1} with pure methanol feed, stable conditions lasted for at least 23 h. The catalyst tested at 550 °C was regenerated in air for 14 h, and the experiment was repeated. The product distribution before and after regeneration was similar indicating that irreversible deactivation was minimal. Samples of the catalyst

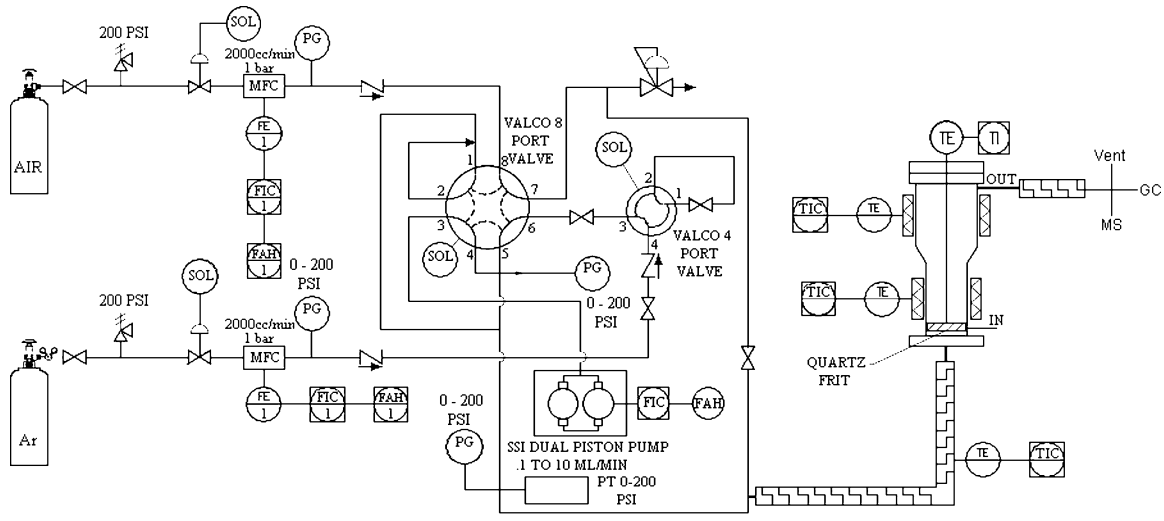

Figure 2. Schematic diagram of the experimental setup.

Table 1. Particle Properties of the Catalyst

$d_p < 45$	0.4	$200 < d_p > 229$	2.9
$45 < d_p < 68$	4.7	$229 < d_p < 262$	1.6
$68 < d_p < 89$	16.6	$262 < d_p < 350$	1.3
$89 < d_p < 102$	15.5	d_p	108 μm
$102 < d_p < 117$	16.7	$\mathbf{u}_{mf}$	0.005 m/s
$117 < d_p < 133$	15.3	ρ_p	1270 kg/m^3
$133 < d_p < 153$	11.9	ρ_{tapped}	855 kg/m^3
$153 < d_p < 175$	8.1	ρ_{mf}	744 kg/m^3
$175 < d_p < 200$	5.0	ε_{mf}	0.405

Table 2. Carbon Deposition on the ZSM-5 Catalyst

temp °C	TOS (h)	wt % carbon	% selectivity to carbon
550	4	0.77	1.38
550	8	1.47	1.33
550	22	4.80	1.67
500	4	0.04	0.07
500	8	0.55	0.49
500	22	1.84	0.61
450	4	0.46	0.82
450	8	1.56	1.41
450	23	1.34	0.42
550[a]	4	0.74	1.32
550[a]	8	1.47	1.33
550[a]	22.5	4.40	1.46

[a] Regenerated catalyst.

were taken from the experiments and the carbon content analyzed by thermogravimetric analysis (TGA). The maximum carbon content detected was 4.8 wt % after 23 h at 550 °C. The results are given in Table 2. The selectivity to carbon was higher at 550 °C where approximately 1.5% of the feed is converted to carbon. At 500 °C, the selectivity to carbon is lower with a maximum value of 0.61%, while at 450 °C the results are scattered. All experiments reported hereafter were conducted over a period of 4−5 h, where the effect of reversible/irreversible deactivation was negligible. Three GC traces were taken for each experiment.

The experimental data are given in Table 3. In experiment no. 20, 100 mL/min of hydrogen was added to the feed gas to investigate the effect of H_2 on the reaction. No change in the product distribution was observed with the addition of hydrogen, that is, hydrogenation of olefins to paraffins was negligible.

Feeding 1-hexene instead of methanol to the catalyst resulted in a product distribution similar to the one obtained for methanol, indicating that cracking and oligomerization are an important part of the reaction scheme. This is also in agreement with the literature, where investigations on the product distribution includes $C_{2=}$ to $C_{10=}$ together with paraffins and aromatics when $C_{3=}$ to $C_{8=}$ and hexane are fed over ZSM-5.[20,22−24] Recently, Zhou et al.[21] have shown that feeding ethylene, propylene, or *n*-butylene over SAPO-34 gives approximately the same product distribution which is close to the thermodynamic equilibrium. As SAPO-34 and ZSM-5 are both acidic catalysts, the reaction mechanism of the light olefins interconversion is likely to be similar, and a similar pattern should be expected for ZSM-5.

Because of the results obtained in the 1-hexene experiment, the work of Norval et al.[25,26] who have studied the equilibrium of the MTG process over ZSM-5, and the recent work of Zhou et al.,[21] it is of interest to establish whether or not the olefins reach equilibrium concentrations. The equilibrium distribution between $C_{2=}$ to $C_{6=}$ have been calculated with HCS Chemistry 5 in the temperature range 400−550 °C where all isomers of the olefins have been considered in the calculations. Figure 3 shows the product distribution and the equilibrium concentrations. The experimental data are far from equilibrium concentrations, especially propylene which is higher than the equilibrium concentration, while the C_4 and C_5 are lower. The trends between the equilibrium calculations and experimental data are in agreement, but the experimental data, with the exception of the C_{6+} fraction, which approaches the calculated values at higher temperatures, suggest that this equilibrium would not be reached in the process. The lighter product distribution could be due to the narrow pores of the ZSM-5 (5.8 Å) which can restrict passage of the heavier components shifting the product distribution toward the lighter components. The equilibrium constants based on the thermodynamic have, therefore, not been used in the kinetic calculations since it would force the reaction toward a heavier product distribution.

Figures 4−6 show the product distribution as a function of time with an equimolar methanol/argon feed at residence times between 2.5 and 6 s. The product distribution is rather constant and full conversion is obtained after 4 s regardless of temperature. The product distribution at each temperature is insensitive to the residence time in the interval investigated. Larger changes are evident with changes in temperature: higher temperatures result in an increase in the ethylene and propylene fractions and a decrease in the higher fractions. The change is largest for ethylene and the C_{6+} fractions. Figure 7 shows the product distribution as a function of residence time with pure methanol feed. At short residence times, the concentration of higher hydrocarbons increases suggesting that they are intermediates.

Table 3. Experimental Results from the Fluid Bed Experiments[a]

expt no.	temp.	MeOH (l) mL/min	Ar (g) mL/min	water (l) mL/min	catalyst g	methane	ethene	ethane	propene	propane	DME	MeOH	C_4	C_5	C_{6+}
1	402	1.84	139.5	0	220	0.43	8.36	0.15	20.35	2.96	3.69	2.49	24.65	16.49	20.43
2	450	1.84	139.5	0	220	0.81	7.75	0.24	29.28	3.36	0.62	0.89	26.03	16.13	14.89
3	500	1.84	139.5	0	220	2.15	12.84	0.67	34.85	3.47	0.00	0.30	23.70	12.16	9.87
4	546	1.84	139.5	0	220	3.93	19.09	1.14	35.49	2.62	0.00	0.10	20.22	6.55	10.87
5	550	0.92	558	0	220	4.22	18.20	0.94	39.02	2.46	0.00	0.09	20.16	9.13	5.78
6	450	0.92	558	0	220	1.04	7.54	0.19	34.11	2.37	0.21	1.40	24.71	15.45	12.99
7	451	3.68	139.5	0	220	0.80	6.09	0.17	30.74	2.04	3.65	3.06	23.58	14.99	14.88
8	450	0.92	0	0.92	220	0.96	6.75	0.17	37.37	1.90	1.36	5.09	22.64	14.24	9.53
9	553	1.84	0	1.84	220	6.12	13.42	0.73	38.27	1.63	0.78	1.87	19.78	11.98	5.42
10	552	1.84	0	0	330	2.91	19.22	1.22	38.45	4.21	0.00	0.07	21.16	8.05	4.71
11	549	1.84	0	1.84	330	2.60	21.71	0.51	40.88	1.76	0.19	0.20	18.48	9.24	4.43
12	550	1.84	1144	0	330	2.85	21.20	0.51	40.17	2.91	0.00	0.04	20.37	8.04	3.91
13	450	1.84	1144	0	330	0.80	9.02	0.16	31.43	3.43	0.09	0.15	27.73	15.35	11.85
14	499	1.84	0	0	330	1.34	11.21	0.46	32.71	4.63	0.01	0.13	27.01	13.97	8.52
15	499	1.84	1144	0	330	1.23	11.96	0.30	38.05	2.78	0.02	0.16	24.04	12.86	8.62
16	502	1.84	0	0	220	2.00	14.14	0.71	34.93	5.52	0.00	0.04	25.92	10.88	5.86
17	500	1.84	1144	0	220	1.17	12.64	0.23	39.51	2.66	0.00	0.15	22.16	10.87	10.60
18	501	0.92	558	0	220	1.62	15.22	0.56	36.57	3.57	0.00	0.11	22.88	10.15	9.32
19	500	0.92	0	0.92	220	1.43	13.26	0.37	41.07	2.62	0.18	0.45	22.40	12.03	6.20
20[b]	500	0.92	558	0	220	1.53	13.28	0.41	37.66	3.17	0.00	0.31	23.18	11.53	8.94
21	500	0.92	558	0	220	1.58	14	0.54	38.35	3.44	0	0.63	23.7	11.39	6.35
22	554	0.92	0	0	220	4.89	22.06	1.71	39.50	2.59	0.00	0.01	19.76	6.04	3.44
24	501	0.92	558	0	110	2.95	15.22	0.34	37.27	1.83	0.42	2.72	20.07	11.55	7.63
25	500	0.92	0	0	110	3.23	15.25	0.58	40.29	2.78	0.00	0.75	22.98	8.73	5.40
26	500	1.68	2288	0	20	0.72	2.63	0.06	20.41	0.31	8.29	25.65	13.69	10.90	17.36
27	453	2.50	0	0	50	0.54	5.64	0.06	26.60	1.35	2.10	6.76	21.53	15.47	19.88
28	501	2.50	0	0	50	0.91	7.14	0.11	35.40	1.34	0.70	3.82	21.78	16.00	12.78
29	550	2.50	0	0	50	3.29	6.98	0.26	31.95	1.06	2.13	5.46	19.68	14.62	14.56
31	500	1.68	0	0	50	0.97	8.21	0.14	33.89	1.78	0.48	2.38	22.46	15.16	14.54
32	501	0.84	0	0	50	0.93	9.33	0.19	32.74	2.32	0.26	1.40	22.49	14.55	15.78
34	502	1.68	2288	0	50	0.84	5.85	0.07	36.23	0.66	2.78	3.11	21.50	15.42	13.54
35	450	0.92	558	0	110	0.95	7.82	0.14	30.29	1.91	0.09	8.24	23.01	13.74	13.81
36	550	0.92	558	0	110	2.56	18.69	0.40	36.89	1.75	0.00	3.13	18.80	8.43	9.34

[a] Product distribution is given in carbon %. [b] Hydrogen (100 mL) was cofeed with methanol and argon.

This was also found in a previous fixed bed study where an increased C_{5+} fraction was observed as the catalyst began to deactivate indicating that they were intermediates.[7]

Fluid-Bed Model. The fluid bed was modeled assuming gas rises predominately in the bubble phase and the reaction takes place in the catalyst in the emulsion phase, with interphase mass transfer between the two. This two phase model is well documented in the literature.[27] The model was used recently by Werther and Hartge[28] to characterize an industrial fluidized-bed reactor and by Abba et al.[29] to describe fluidization from bubbling conditions to fast fluidization. The following assumptions have been made in the model: (1) gas flows only in the axial direction—dispersion in the radial direction is not considered (with the exception of interphase mass transfer); (2) no catalyst in the bubble phase; (3) the activity of the catalyst is considered constant, for instance, no deactivation due to the short reaction time compared to the deactivation time of the catalyst.

The mass balance around the bubble and emulsion phases for the model can be written as

Bubble phase:

$$\frac{\partial(\delta \mathbf{u}_b C_{b,i})}{\partial h} = -\delta K_{be}(C_{b,i} - C_{e,i}) + \Gamma \frac{y_{e,i}}{1 - y_{e,C_x^+}} \quad (1)$$

Emulsion phase:

$$\frac{\partial((1-\delta)\mathbf{u}_{mb} C_{e,i})}{\partial h} = \delta K_{be}(C_{b,i} - C_{e,i}) - \Gamma \frac{y_{e,i}}{1 - y_{e,C_x^+}} + W(-r_i) \quad (2)$$

where Γ is the gas expansion due to reaction which is considered to go to the bubble phase by formation of bubbles in the emulsion phase. The implemented equations are given as follows and a schematic drawing is shown in Figure 8. The equations were discretized using a block element approach with the number of blocks as a parameter; the implemented equations are given in eq 3 and eq 4.

$$0 = -F_{b,n} y_{b,i,n} + F_{b,n-1} y_{b,i,n-1} - \frac{\delta}{1-\delta} V_e K_{be}(C_{b,i,n} - C_{e,i,n}) + \sum_i^N (W_n(-r_i)) \cdot \frac{y_{e,i,n}}{1 - y_{e,C_x^+,n}} \quad (3)$$

$$0 = -F_{e,n} y_{e,i,n} + F_{e,n-1} y_{b,i,n-1} + \frac{\delta}{1-\delta} V_e K_{be}(C_{b,i,n} - C_{e,i,n}) - \sum_i^N (W_n(-r_i)) \cdot \frac{y_{e,i,n}}{1 - y_{e,C_x^+,n}} + W_n(-r_i) \quad (4)$$

Optimization of parameters has been done with the use of the simplex method and the error calculations have been evaluated from eq 5

$$R_i^2 = 1 - \frac{\sum_n^N x_{i,n,\mathrm{expt}}(x_{i,n,\mathrm{calcd}} - x_{i,n,\mathrm{expt}})^2}{\sum_n^N (x_{i,n,\mathrm{expt}} - \bar{x}_{i,\mathrm{expt}})^2} \quad (5)$$

The hydrodynamic correlations used in the fluid-bed calculations are given in Table 4. The mass transfer coefficient correlations used in this work are the ones from Sit and Grace.[30] The bubble diameter has been calculated from the correlation of Mori and Wen.[31] The catalyst belongs to the Geldart A powder classification and the minimum bubbling velocity is therefore used in the correlations for the gas in the emulsion phase. The molecular diffusion coefficient has been estimated to equal 0.4 cm^2/s, based on the average binary diffusion

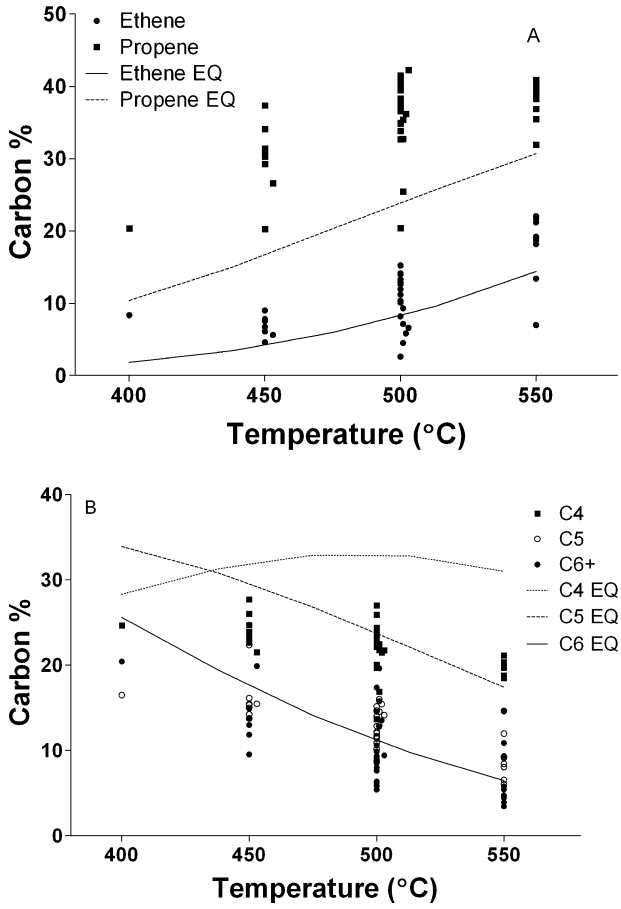

Figure 3. Comparison between experimental MTO data and equilibrium composition of the C2−C6 olefins in the temperature range 400−550 °C: (a) ethylene and propylene, (b) C_4, C_5, C_6.

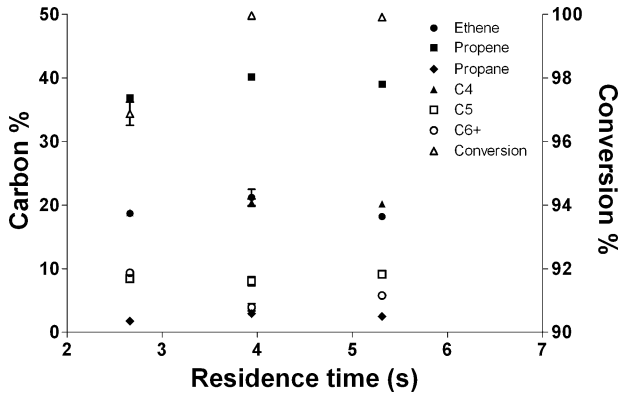

Figure 4. Product distribution vs residence time with methanol/argon feed (molar ratio 1:1) over ZSM-5 at 550 °C.

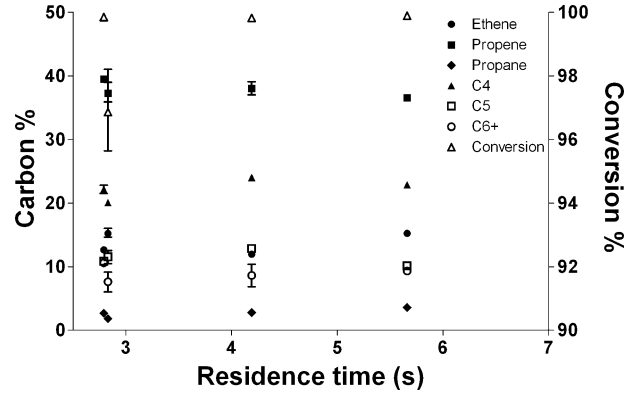

Figure 5. Product distribution vs residence time with methanol/argon feed (molar ratio 1:1) over ZSM-5 at 500 °C.

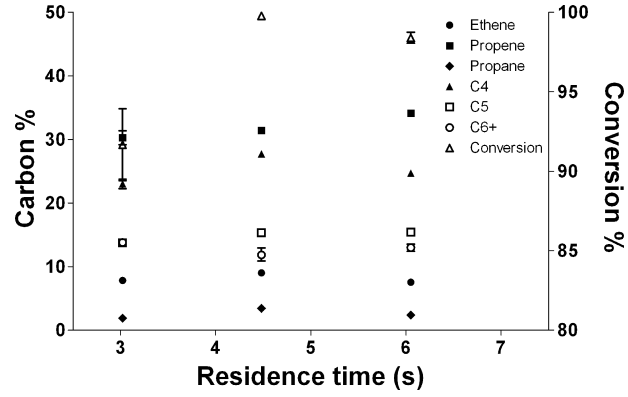

Figure 6. Product distribution vs residence time with methanol/argon feed (molar ratio 1:1) over ZSM-5 at 450 °C.

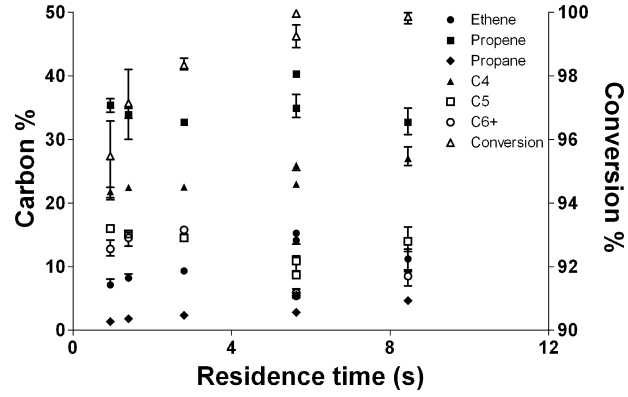

Figure 7. Product distribution vs residence time with pure methanol feed over ZSM-5 at 500 °C.

coefficient between mixtures of methanol, DME, and water. Since a porous plate distributor and relatively low gas velocities are used in the work, the initial bubble size is below 5 mm in the first centimeter of the bed. Therefore, the mass transfer coefficient in the first part of the bed is high and no limitations on the mass transfer are expected. General values of the mass transfer coefficient are in the range of 3−15 s^{-1} at the exit of the bed with the lowest value at the highest gas velocity and catalyst inventory.

Kinetic Model. Several kinetic models have been proposed for the MTO reaction, mostly over ZSM-5 and SAPO zeolites.[5,8,9,14,17−19,34−36] The main difference in the models based on ZSM-5 and SAPO is the addition of C_6^+ compounds in the models with the ZSM-5 zeolite. Further, it has been shown through ^{13}C experiments that the catalytically active reaction intermediates in ZSM-5 and SAPO-34 are somewhat different.[37,38] Transient $^{12}C/^{13}C$ methanol conversion studies on ZSM-5 showed that, upon switching from $^{12}CH_3OH$ to $^{13}CH_3OH$, the ^{13}C content of ethylene closely follows that of the aromatics and that the higher olefins, to a considerable extent, are formed from methylation and interconversion.

The experiments with 1-hexene in argon over ZSM-5, previously described, have shown that the product distribution is quite similar to the product distribution with pure methanol feed. Figure 9 shows the product distribution of experiments made with methanol and 1-hexene diluted in argon feed over ZSM-5 catalyst with constant inlet flow rate. The product

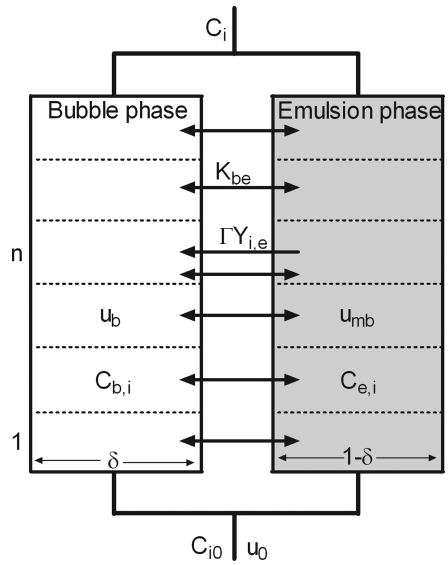

Figure 8. Schematic drawing of the fluid bed model.

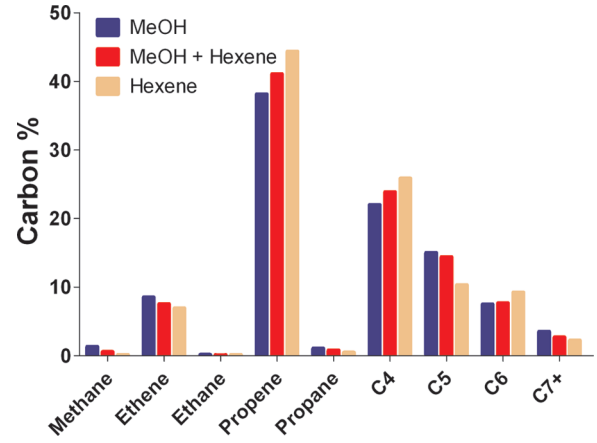

Figure 9. Product distribution of reaction over ZSM-5 with three different feed compositions and a total inlet flow rate of 1.57 L/min at 500 °C: (1) methanol/argon molar ratio 1:2 (2) methanol/1-hexene/argon molar ratio 9:1:20 and (3) 1-hexene/argon molar ratio 1:2.

distributions are similar, although there are some changes in the individual olefin fractions. Feeding 1-hexene yields slightly more propylene, butylenes, and hexenes compared to feeding methanol and less of the other olefins. Methane is formed from methanol/DME and not from the olefin reactions which also have been found from fixed-bed experiments.[25] Propane and aromatic compounds are also observed in the exit gas with 1-hexene but to a lesser degree than with methanol.

On the basis of the product distribution of the experiments with methanol and 1-hexene feed, the product distribution looks like it is highly dependent on the cracking and oligomerization reactions and the exact route from methanol to hydrocarbons might therefore not be crucial to the product distribution. A route from higher olefins to ethylene and propylene should also be included in the kinetics, which in most cases is not present in the current available models.

The kinetics of the MTO reaction are complicated, involving oxygenates, paraffins, olefins and aromatics, with the main components being the light olefins ethylene and propylene. The kinetic model is developed to enable the prediction of the main fractions of the MTO process. Ethylene and propylene are taken as individual components while the olefins and paraffins in the C_4 and C_5 fractions are lumped together.

The kinetic scheme that has been used to model the reaction is based on fast reaction between methanol and DME to give an equilibrium composition. Methanol and DME react through the hydrocarbon pool mechanism and subsequent homologation/oligomerization reactions to form higher olefins (C_x^+), in this model represented by a single component,

Table 4. Hydrodynamic Correlations

variable	correlation	ref
mass transfer coefficient	$k_{be} = \frac{\mathbf{u}_{mb}}{3} + \left(\frac{4D\varepsilon_{mf}\bar{u}_b}{\pi\bar{d}_b}\right)^{1/2}, \quad K_{be} = \frac{6k_{be}}{d_b}$	Sit and Grace[30]
bubble diameter	$d_b = d_{bm} - (d_{bm} - d_{b0})\exp\left(\frac{-0.3h}{D_t}\right)$ (cm) $d_{b0} = 0.00376(\mathbf{u}_0 - \mathbf{u}_{mb})^2, \quad d_{bm} = 0.652(A_t(\mathbf{u}_0 - \mathbf{u}_{mb}))^{0.4}$	Mori and Wen[31]
bubble velocity	$\mathbf{u}_b = \mathbf{u}_0 - \mathbf{u}_{mb} + 0.711(gd_b)^{1/2}$	
minimum fluidization velocity	$\mathbf{u}_{mf} = \frac{\mu}{d_p\rho_g}\left[\left[(33.7)^2 + 0.0408\left(\frac{d_p^3\rho_g(\rho_s - \rho_g)g}{\mu^2}\right)\right]^{1/2} - 33.7\right]$	Wen and Yu[32]
minimum bubbling	$\frac{\mathbf{u}_{mb}}{\mathbf{u}_{mf}} = \frac{2300\rho_g^{0.126}\mu^{0.523}\exp(0.716F)}{d_p^{0.8}g^{0.934}(\rho_p - \rho_g)^{0.934}}$	Abrahamsen and Geldart[33]
bubble fraction	$\delta = \frac{\mathbf{u}_0 - \mathbf{u}_{mb}}{\mathbf{u}_b - \mathbf{u}_{mb}}$	

Table 5. Kinetic Model with Optimized Parameters for k_0 (Arrhenius Equation without a Reference Temperature) and Activation Energy k

no.	reaction	reaction rate	k_0	k (m^3/(kg·s))	E_a (kcal/mol)
1	$2CH_3OH \leftrightarrow C_2H_5OH$	considered in equilibrium			
2	$10CH_3OH \rightarrow C_x^+ + 10H_2O$	$-r_2 = k_2 C_{MeOH} Z$	1.7	2.83×10^{-2}	6.28
3	$5C_2H_5OH \rightarrow C_x^+ + 5H_2O$	$-r_3 = k_3 C_{DME} Z$	9	4.43×10^{-4}	15.2
4	$C_x^+ \rightarrow 5C_2H_4$	$-r_4 = k_4 C_{C_x^+} z$	2.70×10^5	0.508	20.2
5	$5C_2H_4 \rightarrow C_x^+$	$-r_5 = k_5 C_{C_2H_4} Z$	14.6	1.63×10^{-5}	21.0
6	$C_x^+ \rightarrow \frac{10}{3}C_3H_6$	$-r_6 = k_6 C_{C_x^+} z$	2.76×10^3	1.56	11.46
7	$\frac{10}{3}C_3H_6 \rightarrow C_x^+$	$-r_7 = k_7 C_{C_3H_6} Z$	65.0	2.05×10^{-4}	19.41
8	$C_x^+ \rightarrow 2.5C_4H_8$	$-r_8 = k_8 C_{C_x^+} z$	87.1	0.940	6.94
9	$2.5C_4H_8 \rightarrow C_x^+$	$-r_9 = k_9 C_{C_4H_8} Z$	0.23	2.31×10^{-5}	14.12
10	$C_x^+ \rightarrow 2C_5H_{10}$	$-r_{10} = k_{10} C_{C_x^+} z$	0.73	0.467	0.69
11	$2C_5H_{10} \rightarrow C_x^+$	$-r_{11} = k_{11} C_{C_5H_{10}} Z$	1.33×10^{-4}	1.03×10^{-5}	3.92
12	$C_x^+ \rightarrow \frac{5}{3}C_6H_{12}$	$-r_{12} = k_{12} C_{C_x^+} z$	2.52	0.893	1.59
13	$\frac{5}{3}C_6H_{12} \rightarrow C_x^+$	$-r_{13} = k_{13} C_{C_6H_{12}} Z$	13.5	2.44×10^{-3}	5.23
14	$6C_3H_6 \rightarrow C_9H_{12} + 3C_3H_8$	$-r_{14} = k_{14} C_{C_3H_6} Z$	1.11×10^{-4}	4.23×10^{-5}	1.48
15	$2CH_3OH \rightarrow CH_4 + C + 2H_2O$	$-r_{15} = k_{15} C_{MeOH} Z$	3.46	1.11×10^{-2}	8.80

[a] Calculated with a reference temperature of 500°C.

decene. C_x^+ is considered to react to each of the C_2-C_6 olefins through reversible reactions. The C_x^+ is treated as a component related to the catalyst and therefore only present in the emulsion phase.

Reactions for the formation of aromatics have been taken into account and are assumed to form from propylene and the excess hydrogen goes to the formation of paraffins. The aromatic compound in this work is taken as trimethylbenzene and the paraffin as propane. Methane is assumed to be formed directly from methanol or DME and the excess carbon arising in the reaction from methanol to methane is assumed to go to carbon formation, since CO and CO_2 were not detected in appreciable amounts that could justify reaction to these components. The carbon formation from this reaction is, however, above the quantities measured by TGA (Table 2) which could indicate a different route to methane. All reactions with the exception of the MeOH/DME equilibrium have been regarded as first order reactions and the influence of water have also been taken into account the reactions are listed in Table 5 a schematic drawing is shown in Figure 10.

The influence of water in the kinetics is taken into account in terms of equation 6; the constants in K_w have been found by optimization. In the experiments Z is in the range 0.8−1, indicating that the effect of water is relatively low. However,

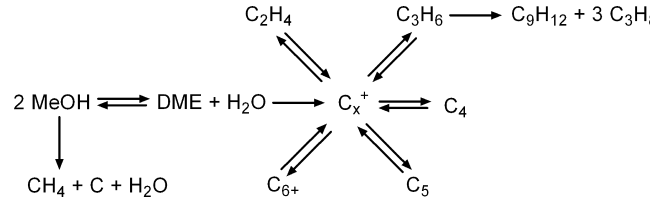

Figure 10. Schematic drawing of the kinetic model.

including the Z term does improve the predictions especially at higher water concentrations, for example, when water is cofed.

$$Z = \frac{1}{(1 + K_w C_w)} \text{ where } K_w = 3.6 \exp\left[\frac{-12.1}{R}\left(\frac{1}{T} - \frac{1}{T_0}\right)\right] \quad (6)$$

The temperature dependency of the reactions is taken into account with the Arrhenius equation with a reference temperature of 500 °C.

$$k = k^* \exp\left[\frac{-E_a}{R}\left(\frac{1}{T} - \frac{1}{T^*}\right)\right] \quad (7)$$

Modeling Results. The parameters in the model were estimated by minimizing eq 5 with simplex. The k^* and E_a values were optimized simultaneous with a reference temper-

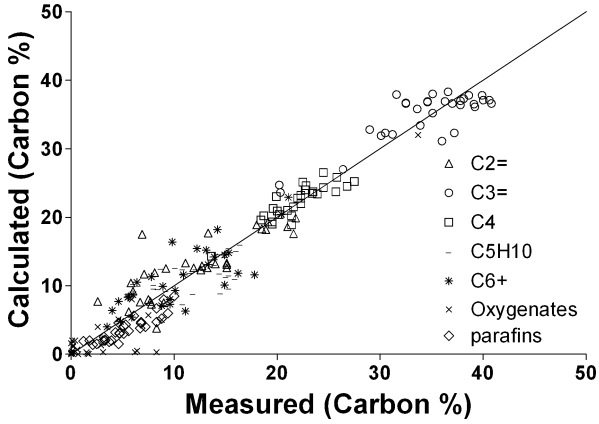

Figure 11. Comparison of the calculated product distribution to the measured data.

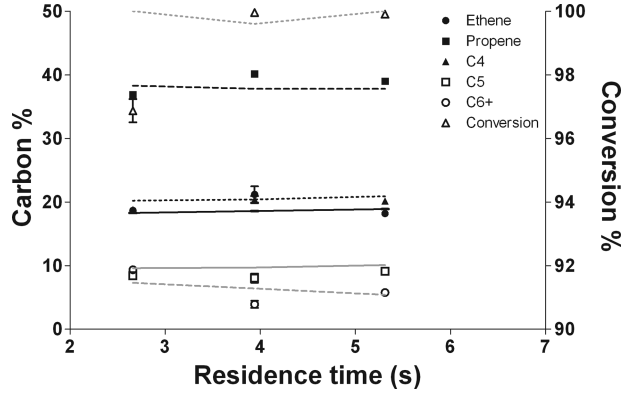

Figure 12. Measured (points) and calculated (lines) data at 550 °C with methanol/argon (ratio 1:1) feed as a function of residence time in the fluid bed: (Δ, ⋯) conversion; (●, —) ethylene; (■, ---) propylene; (▲, ⋯) C_4; (□, —) C_5; (○, ---) C_{6+}.

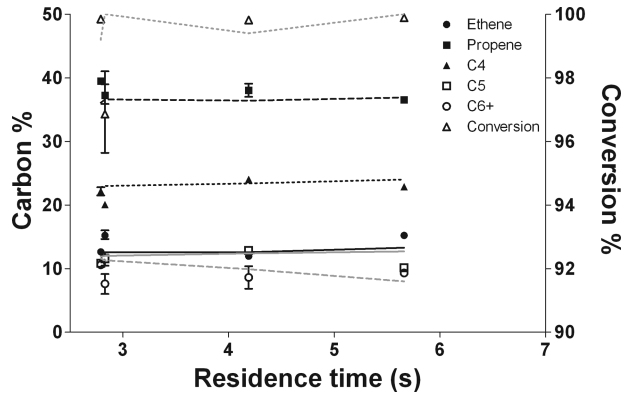

Figure 13. Measured (points) and calculated (lines) data at 500 °C with methanol/argon feed (ratio 1:1) as a function of residence time in the fluid bed: (Δ, ⋯) conversion; (●, —) ethylene; (■, ---) propylene; (▲, ⋯) C_4; (□, —) C_5; (○, ---) C_{6+}.

ature of 500 °C. Since the C_{6+} fraction was measured as a lump fraction and aromatics were not measured specifically, the C_{6+} and aromatic fractions in the model account for the total measured C_{6+} fraction. The reaction of methanol to DME is considered to be in equilibrium owing to high reaction rate at the reaction temperature. The results are presented in Table 5. The rate constants from decene to olefins at 500 °C are generally 4−5 orders of magnitude higher than the reverse reaction. Furthermore, the reaction from methanol to decene is approximately 10 times faster than from hexene to decene. Calculations of the 1-hexene experiments with the obtained

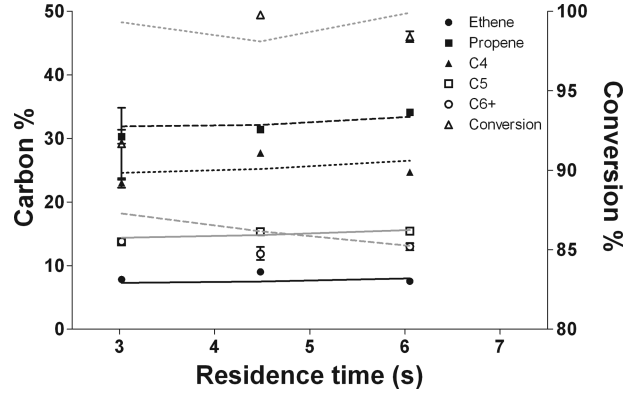

Figure 14. Measured (points) and calculated (lines) data at 450 °C with methanol/argon feed (ratio 1:1) as function of residence time in the fluid bed: (Δ, ⋯) conversion; (●, —) ethylene; (■, ---) propylene; (▲, ⋯) C_4; (□, —) C_5; (○, ---) C_{6+}.

kinetics shows only 11% 1-hexene conversion versus the 89% conversion observed during the experiment. It is evident that the model does not accurately describe the cracking of the higher olefinic species and further investigation into this part of the kinetic model is needed for a more accurate description.

The activation energy values of the C_x^+ to olefin reactions decreases with an increase in olefin molecular weight. This agrees with experimental findings where increasing temperatures leads to higher concentrations of the lower olefins. The values of the activation energies are higher than the values reported by Gayubo et al.[17] which were in the range of 55−70 kJ/mol for ethylene and propylene and 20−25 kJ/mol for the higher olefins. Their work was based on SAPO catalyst and the difference in the active sites on the catalyst compared to the ZSM-5 might influence the activation energies to some extent.

Looking at the difference in the forward and backward reaction rate constants for the reaction of the olefin intermediate, C_x^+, to the lower olefins, it is clear that the reverse reaction rate constants are much lower indicating a very low concentration of the hydrocarbon pool species. Zhou et al.[21] have reported reaction rate constants for similar reactions in a SAPO catalyst at 450 °C, and they reported that the reaction rate constants were all of the same order of magnitude. The large difference could be attributed to a larger fraction of higher components that remain in the pores in the SAPO catalyst, compared to the ZSM-5.

The calculated and experimental data are compared in Figure 11. The model captures the overall trends quite well but requires improvements to simulate the species concentrations. The model is poor in representing the trends for the C_{6+}, paraffin fractions, and oxygenate conversion. Figures 12−14 compare the experimental data and the calculations with methanol/argon feed at three different temperatures. Overall, the calculations of the olefins are in agreement with the experimental data with the exception of the C_{6+} fraction. This could be because the C_{6+} fraction lumps both aromatics and large olefins. The mechanism for these fractions most certainly are different and therefore require separate kinetics. However, they only represent a small fraction of the overall product. The different kinetics pertaining to the formation of aromatics and large olefins could also account for the different trend in the C_{6+} fraction compared to the C_4 and C_5 during the equilibrium calculations. Figure 15 shows the calculated and measured data at 500 °C with a feed consisting of pure methanol. The same trends as for the methanol/argon feed are observed. Overall, the model is able

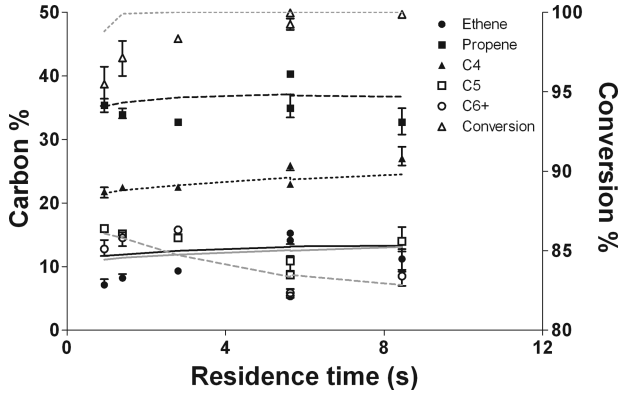

Figure 15. Measured (points) and calculated (lines) data at 500 °C with methanol feed ratio 1:1 as function of residence time in the fluid bed: (Δ, ⋯) conversion; (●, —) ethylene; (■, ---) propylene; (▲, ⋯) C_4; (□, —) C_5; (○, ---) C_{6+}.

to fit the experimental data fairly well from 450 to 550 °C especially with respect to the main olefin species.

Conclusions

Experimental data for the MTO reaction in a fluidized bed show that methanol and 1-hexene feed yield approximately the same product distribution. Methane formation is almost nonexistent with 1-hexene feed compared to methanol feed indicating that methane is predominately formed from oxygenates. When oxygenates are converted to hydrocarbons, they follow the same reaction mechanism as with 1-hexene feed and the olefin composition approaches an equilibrium composition. Equilibrium calculations, however, show that much less light olefins and more high olefins should be produced. This could be due to the narrow pores in the ZSM-5 which could allow easier passage for the light olefins out of the catalyst thus shifting the product distribution toward lower molecular weight species.

A model for the MTO reaction over ZSM-5 is proposed. The model involves 15 reactions where all olefins are formed in equilibrium, inside pores and intersections, through a common large olefinic intermediate. The model predicts the experimental data fairly well for the olefins but requires improvements with respect to the paraffin and C_{6+} fractions.

Nomenclature

A_t = cross-sectional area of the fluid bed (m^2)
C = molar concentration ($kmol/m^3$)
C_x^+ = hydrocarbon pool species (decene)
D = molar diffusion coefficient (m^2/s)
D_t = reactor diameter (m)
d_p = particle diameter (m)
d_b = bubble diameter (m)
d_{b0} = initial bubble diameter at the distributor (m)
d_{bm} = maximum bubble diameter (m)
E_a = activation energy (kJ/mol)
F = fine fraction
F = flow rate (kmol/s)
g = gravity (m/s^2)
h = height in bed (m)
K_{eq} = equilibrium constant
k_i = reaction rate constant ($m^2/(kg \cdot s)$)
k_0 = reaction rate constant Arrhenius eq without reference temperature ($m^2/(kg \cdot s)$)
K_{be} = bubble to emulsion mass transfer coefficient (s^{-1})
k_{be} = bubble to emulsion mass transfer coefficient (m/s)
N = total number of components in the system
r_i = reaction rate of component i ($kmol/(kg \cdot s)$)
R = ideal gas constant ($kcal/(mol \cdot K)$)
T = temperature (K)
$\mathbf{u}_{mf}$ = minimum fluidization velocity (m/s)
$\mathbf{u}_{mb}$ = minimum bubbling velocity (m/s)
$\mathbf{u}_b$ = bubble velocity (m/s)
$\mathbf{u}_0$ = superficial gas velocity (m/s)
V_e = volume of emulsion (m^3)
W = catalyst weight (kg)
y = mole fraction

Greek Symbols

Γ = gas expansion due to reaction
δ = bubble phase volumetric fraction
ε_{mf} = void fraction at minimum fluidization
ε_{cat} = void fraction of the catalyst
μ = gas viscosity ($kg/(m \cdot s)$)
ρ_p = particle density (kg/m^3)
ρ_b = bulk density (kg/m^3)
ρ_{tapped} = tapped density (kg/m^3)
ρ_{mf} = minimum fluidization density (kg/m^3)
ρ_g = gas density (kg/m^3)

Subscripts

e = emulsion phase
b = bubble phase
i = component index
n = CSTR in series
expt = experimental data
calcd = calculated value

Literature Cited

(1) Chang, C. D.; Silvestri, A. J. The Conversion of Methanol and Other O-Compounds to Hydrocarbons over Zeolite Catalysts. *J. Catal.* **1977**, *47*, 249.

(2) Stöcker, M. Methanol-to-Hydrocarbons: Catalytic Materials and Their Behaviour. *Microporous Mesoporous Mater.* **1999**, *29*, 3.

(3) Chang, C. D.; Chu, C. T-W. Methanol Conversion to Olefins over ZSM-5. II. Olefin Distribution. *J. Catal.* **1984**, *86*, 297.

(4) Park, T-Y.; Froment, G. F. Kinetic Modeling of the Methanol to Olefins Process. 2. Experimental Results, Model Discrimination, and Parameter Estimation. *Ind. Eng. Chem. Res.* **2001**, *40*, 4187.

(5) Gayubo, A. G.; Anuayo, A. T.; Olazar, M.; Vivanco, R.; Bilbao, J. Kinetics of the Irreversible Deactivation of the HZSM-5 Catalyst in the MTO Process. *Chem. Eng. Sci.* **2003**, *58*, 5239.

(6) Mier, D.; Aguayo, A. T.; Atutxa, A.; Gayubo, A. G.; Bilbao, J. Kinetic Study of the Simultaneous Cracking of Paraffins and Methanol on HZSM-5 Zeolite Catalyst. *Int. J. Chem. Reactor Eng.* **2007**, *5*, A60.

(7) Kaarsholm, M.; Joensen, F.; Nerlov, J.; Cenni, R.; Chaouki, J.; Patience, G. S. Phosphorus Modified ZSM-5: Deactivation and Product Distribution for MTO. *Chem. Eng. Sci.* **2007**, *62*, 5527.

(8) Gayubo, A. G.; Aguayo, A. T.; Alonso, A.; Bilbao, J. Kinetic Modeling of the Methanol-to-Olefins Process on a Silicoaluminophosphate (SAPO-18) Catalyst by Considering Deactivation and the Formation of Individual Olefins. *Ind. Eng. Chem. Res.* **2007**, *46*, 1981.

(9) Schoenfelder, H.; Hinderer, J.; Werther, J.; Keil, F. J. Methanol-to-Olefins—Predictions of the Performance of a Circulating Fluidized-Bed Reactor on the Basis of Kinetic Experiments in a Fixed-Bed Reactor. *Chem. Eng. Sci.* **1994**, *49*, 5377.

(10) Keil, F. J. Methanol-to-Hydrocarbons: Process Technology. *Microporous Mesoporous Mater.* **1999**, *29*, 49.

(11) Chen, J. Q.; Bozzano, A.; Glover, B.; Fuglerud, T.; Kvisle, J. Recent Advancements in Ethylene and Propylene Production Using the UOP/Hydro MTO Process. *Catal. Today.* **2005**, *106*, 103.

(12) Mihail, R.; Straja, S.; Maria, G.; Musca, G.; Pop, G. Kinetic Model for Methanol Conversion to Hydrocarbons. *Chem. Eng. Sci.* **1983**, *38*, 1581.

(13) Park, T-Y.; Froment, G. F. Kinetic Modeling of the Methanol to Olefins Process. 1. Model Formulation. *Ind. Eng. Chem. Res.* **2001**, *40*, 4172.

(14) Park, T-Y.; Froment, G. F. Kinetic Modeling of the Methanol to Olefins Process. 2. Experimental Results, Model Discrimination, and Parameter Estimation. *Ind. Eng. Chem. Res.* **2001**, *40*, 4187.

(15) Gayubo, A. G.; Aguayo, A. T.; Castilla, M.; Olazar, M.; Bilbao, J. Catalyst Reactivation Kinetics for Methanol Transformation into Hydrocarbons. Expressions for Designing Reaction-Regeneration Cycles in Isothermal and Adiabatic Fixed Bed Reactor. *Chem. Eng. Sci.* **2001**, *56*, 5059.

(16) Gayubo, A. G.; Aguayo, A. T.; Castilla, M.; Moran, A. L.; Bilbao, J. Role of Water in the Kinetic Modelling of Methanol Transformation into Hydrocarbons on HZSM-5 Zeolite. *Chem. Eng. Commun.* **2004**, *191*, 944.

(17) Gayubo, A. G.; Aguayo, A. T.; Sánchez del Campo, A. E.; Tarrio, A. M.; Bilbao, J. Kinetic Modelling of Methanol Transformation into Olefins on a SAPO-34 Catalyst. *Ind. Eng. Chem. Res.* **2000**, *39*, 292.

(18) Park, T-Y.; Froment, G. F. Analysis of Fundamental Reaction Rates in the Methanol-to-Olefins Process on ZSM-5 as a Basis for Reactor Design and Operation. *Ind. Eng. Chem. Res.* **2004**, *43*, 682.

(19) Bos, R. A. N.; Tromp, P. J. J.; Akse, H. N. Conversion of Methanol to Lower Olefins. Kinetic Modelling, Reactor Simulation, and Selection. *Ind. Eng. Chem. Res.* **1995**, *34*, 3808.

(20) Buchanan, J. S.; Santiesteban, J. G.; Haag, W. O. Mechanistic Considerations in Acid-Catalyzed Cracking of Olefins. *J. Catal.* **1996**, *158*, 279.

(21) Zhou, H.; Wang, Y.; Wei, F.; Wang, D.; Wang, Z. Kinetics of the Reactions of the Light Alkenes over SAPO-34. *Appl. Catal., A* **2008**, *348*, 135.

(22) Tabak, S. A.; Krambeck, F. J.; Garwood, W. E. Conversion of Propylene and Butylene over ZSM-5 Catalyst. *AIChE J.* **1986**, *32* (9), 91526.

(23) Lukyanov, D. B.; Shtral, V. I.; Khadzhiev, S. N. A Kinetic Model for the Hexane Cracking Reaction over H-ZSM-5. *J. Catal.* **1994**, *146*, 87.

(24) Norval, G. W.; Phillips, M. J.; Virk, K. S.; Simons, R. V. Olefin Conversion over Zeolite H-ZSM-5. *Can. J. Chem. Eng.* **1987**, *67*, 521.

(25) Norval, G. W.; Phillips, M. J.; Missen, R. W.; Smith, W. R. Identification and Application of Partial Chemical Equilibria in Reactor Modeling. *AIChE J.* **1992**, *38*, 1288.

(26) Norval, G. W.; Phillips, M. J.; Missen, R. W.; Smith, W. R. Calculated Equilibria for the Alkene and Alcohol Aromatization Processes. *Appl. Catal.* **1989**, *54*, 37.

(27) Kunii, D.; Levenspiel, O. *Fluidization Engineering;* Butterworth-Heinemann: Newton, MA, 1991.

(28) Werther, J.; Hartge, E.-U. Modeling of Industrial Fluidized-Bed Reactors. *Ind. Eng. Chem. Res.* **2004**, *43*, 5593.

(29) Abba, I. A.; Grace, J. R.; Bi, H. T.; Thompson, M. L. Spanning the Flow Regimes: Generic Fluidized-Bed Reactor Model. *AIChE J.* **2003**, *49*, 1838.

(30) Sit, S. P.; Grace, J. R. Effect of Bubble Interaction on Interphase Mass Transfer in Gas Fluidized Beds. *Chem. Eng. Sci.* **1981**, *36*, 327.

(31) Mori, S.; Wen, Y. Estimation of Bubble Diameter in Gaseous Fluidized Beds. *AIChE J.* **1975**, *21* (1), 109.

(32) Wen, C. Y.; Yu, Y. H. Mechanics of Fluidization. *Chem. Eng. Progr. Symp.* **1966**, *62*, 100.

(33) Abrahamsen, A. R.; Geldart, D. Behaviour of Gas-Fluidized Beds of Fine Powders Part 1. Homogeneous Expansion. *Powder Technol.* **1980**, *26*, 35.

(34) Alwahabi, S. M.; Froment, G. F. Conceptual Reactor Design for the Methanol-to-Olefins Process on SAPO-34. *Ind. Eng. Chem. Res.* **2004**, *43*, 5112.

(35) Iordache, O. M.; Maria, G. C.; Pop, G. L. Lumping Analysis for the Methanol Conversion to Olefins Kinetic Model. *Ind. Eng. Chem. Res.* **1988**, *27*, 2218.

(36) Soundararajan, S.; Dalai, A. K.; Berruti, F. Modeling of Methanol-to-Olefins (MTO) Process in a Circulation Fluidized-Bed Reactor. *Fuel.* **2001**, *80*, 1187.

(37) Bjørgen, M.; Svelle, S.; Joensen, F.; Nerlov, J.; Kolboe, S.; Bonino, F.; Palumbo, L.; Bordiga, S.; Olsbye, U. Conversion of Methanol to Hydrocarbons over Zeolite H-ZSM-5: On the Origin of the Olefinic Species. *J. Catal.* **2007**, *249*, 195.

(38) Svelle, S.; Joensen, F.; Nerlov, J.:; Olsbye, U.; Lillerud, K-P.; Kolboe, S.; Bjørgen, M. Conversion of Methanol into Hydrocarbons over Zeolite H-ZSM-5: Ethene Formation Is Mechanistically Separated from the Formation of Higher Alkenes. *J. Am. Chem. Soc.* **2006**, *128*, 14770.

Received for review March 1, 2009
Revised manuscript received October 24, 2009
Accepted November 4, 2009

IE900341T